Silicon (2022) 14:9061–9070
https://doi.org/10.1007/s12633-021-01555-w

ORIGINAL PAPER

Device Physics Based Analytical Modeling and Simulation Study of Electrical Characteristics of ISFET pH-sensor

Dayananda Khwairakpam[1] · Puspa Pukhrambam[1] · Vandana Wangkheirakpam[1]

Received: 1 September 2021 / Accepted: 15 November 2021 / Published online: 22 January 2022
© The Author(s), under exclusive licence to Springer Nature B.V. 2021

Abstract
In this article, an analytical framework is put together to describe a pH Sensor based on Ion Sensitive Field-Effect Transistor (ISFET) and then simulated using Synopsys TCAD tool. In the proposed simulation work the electrolyte material and oxide surface charge density have been modeled explicitly by using experimental data available in the literature which makes this study unique from previously reported works. Furthermore, the method for adding a new material in Synopsys TCAD and using its advanced PMI feature are briefly illustrated in this work. The proposed work is validated against an available experimental work with good accuracy of 2.66% error percentage in the result. This article gives an adequate insight into the working principle of ISFET device with the objective of assisting beginners in this field before one can proceed into advanced research.

Keywords ISFET · Matlab · pH-Sensor · PMI · Simulation · TCAD

1 Introduction

A chemical sensor is a transducer linking the chemical domain to the electrical domain. Its response should be fast and selective for the analyte species in interest. A traditional pH sensor having glass electrode is bulky and fragile in nature with difficulty in miniaturization [1]. Ion-Sensitive Field Effect Transistor (ISFET) gives the idea of lab-on-chip system having multiple biosensors mounted on the same chip designed for various applications like soil analysis, waste water analysis and so on [2–4]. In order to understand the basic working principle governing an ISFET device, we've considered a simple pH sensor based on a long channel device without any appreciable short channel effects (SCEs) to be most suited for the purpose.

✉ Dayananda Khwairakpam
dayananda.ece.bmsce@gmail.com

Puspa Pukhrambam
puspa.devi@ece.nits.ac.in

Vandana Wangkheirakpam
vannawang46@gmail.com

[1] ECE Department, NIT Silchar, Cachar, 788010, Assam, India

The basic principle of an ISFET pH-sensor is removing the metal gate of a MOSFET structure and expose the surface of oxide layer directly to the electrolyte solution whose pH change is to be detected. Then a reference electrode is placed into the electrolyte against which the drain current characteristic is to be plotted [1]. The Site-Binding model [5] proposes that atoms on the oxide surface become amphoteric when they come in contact with the electrolyte solution i.e. they release protons into the soultion and become negatively charged or accept protons from the solution and become positively charged or simply remain as neutral sites. These surface reactions depend on the number of binding sites (Ns) and dissociation constants, Ka and Kb (acidity and basicity constants) specific to the oxide surface as well as the concentration of hydronium and hydroxide ions in the electrolyte—the pH value The electrolyte-oxide interface and the oxide-semiconductor interface act like a parallel plate capacitor. Hence, a positive (or negative) charge density developed on the electrolyte-oxide interface is balanced out by a negative (or positive) charge density at the other interface. This in turn modulates the surface potential over the device channel according to the pH value, thereby affecting the drain current characteristic.

This article reviews the previous studies [1, 2, 5–11] and compiles a compact analytical model governing the ISFET pH sensor as shown in Section 2. This section would help beginners such as myself in understanding the

physics governing the ISFET device. The analytical model is then solved using MATLAB [12–15] to keep a theoretical reference. Section 3 describes the TCAD simulation of the proposed structure, with certain alterations to the methods used in previous work [16] — N_C and N_V are considered to be different in the case of a pH sensor, PMI models employed for interface traps are implemented between the stern-layer and the electrolyte, and user-defined models are designed explicitly using available experimental data from [9, 17–21]. TCAD simulation is demonstrated in Section 3 with the help of [22–28]. Validation of the simulation results is done against the experimental data in [29] and also with reference to the theoretical data obtained from MATLAB. The effects caused inside the ISFET structure due to the pH change are also demonstrated using Sentaurus Visual and analyzed in Section 4. Conclusion is then summarized in Section 5 along with future work.

2 Analytical Framework

2.1 Model Formulation

The concept of Double Layer (DL) [8] is used in our approach. DL is a structure having two parallel layers of charge that appears on the oxide surface when it gets exposed to an ionic solution. The first layer consists of ions adsorbed onto the oxide surface as a result of chemical interactions. This layer is referred to as the stern layer. The second layer consists of the ions attracted to the first layer surface charge via Coulombic force, and electrically screens the first layer [8].

Figure 1 shows the 2D schematic of ISFET displaying the various potential drops across it. This structure is used

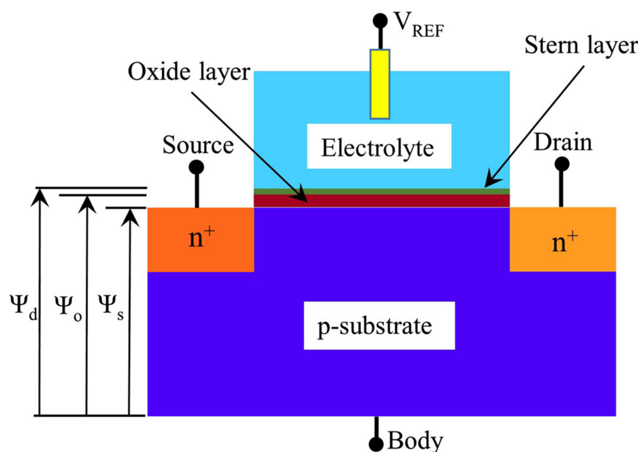

Fig. 1 Schematic structure of an ISFET pH sensor. V_{REF} is applied at the reference gate electrode, Ψ_d is the potential developed over the stern layer while Ψ_o is developed over the oxide surface and Ψ_s is the surface potential induced at the oxide-semiconductor interface

to develop an analytical model governing the Electrolyte-Insulator-Semiconductor (EIS) system. The principle of conservation of charge dictates that the distribution of total charge densities across the EIS system must be zero, i.e.

$$\sigma_d + \sigma_o + \sigma_{mos} = 0 \tag{1}$$

where σ_d is the charge density across the stern layer, σ_o is the charge density on the oxide surface, and σ_{mos} is the charge density inside the semiconductor. By examining Fig. 1, σ_d can be expressed [10] in terms of Ψ_o as:

$$\sigma_d = (\Psi_d - \Psi_o)C_{stern} \tag{2}$$

where C_{stern} is the capacitance across the stern layer whose value is determined to be $20F/cm^2$ [16]. According to Gouy-Chapman Theory [13], by solving Poisson equation in the diffuse region of the electrolyte, the charge density σ_d can be expressed in terms of Ψ_d as follows:

$$\sigma_d = \sqrt{8\varepsilon_0\varepsilon_w kTc_0}sinh\left[(-q\Psi_d)/(2kT)\right] \tag{3}$$

ε_w is the dielectric constant of the electrolyte solution, whose value is taken as that of water, and c_o is the ion concentration in the electrolyte whose value is considered in such a way that only hydronium and hydroxide ions make up the total ion concentration. The Site-Binding Model [5] describes the charging mechanism of the oxide surface. Accordingly, σ_o is described as:

$$\sigma_o = qN_s\left(\frac{[H_S^+]^2 - K_aK_b}{[H_S^+]^2 + K_aK_b + K_b[H_S^+]}\right) \tag{4}$$

where $[H_S^+]$ is the hydrogen ion concentration and the values of Ns, K_a and K_b are taken from [16]. The relation between the hydrogen ion concentration at the surface $[H_S^+]$ and the hydrogen ion concentration inside the electrolyte bulk $[H_B^+]$ is given by the Boltzmann equation [10]:

$$[H_S^+] = [H_B^+]exp\left(-\frac{q\Psi_o}{kT}\right) \tag{5}$$

$[H_B^+]$ can be easily calculated from the pH of the solution [15] using a relation given by $pH = -log_{10}[H_B^+]$. From Fig. 1, we can derive the third type of charge density, σ_{mos} in terms of Ψ_o as follows:

$$\sigma_{mos} = (\Psi_s - \Psi_o)C_{ox} \tag{6}$$

C_{ox} is the oxide capacitance of the MOSFET. According to [14], the charge density developed inside the semiconductor under the oxide can be approximated as:

$$\sigma_{mos} = -\sqrt{2q\varepsilon_{Si}\varepsilon_0 N_A}\sqrt{\Psi_s + \phi_t e^{\frac{\Psi_s - 2\phi_F}{\phi_t}}} \tag{7}$$

q is the charge of an electron, ε_{Si} is the relative permittivity of silicon, N_A is the p-substrate dopant concentration, ϕ_t is the thermal voltage at 300K, ϕ_F is the fermi potential of the semiconductor. σ_{mos} is taken to be negative since we consider an n-channel MOSFET whose

surface potential Ψ_s is positive. According to [14], for the channel to be in moderate to strong inversion, ϕ_F value should be approximately $13\phi_t$ for N_A equal to $10^{16}cm^{-3}$ and Ψ_s should be around $2\phi_F + 6\phi_t$ [14].

2.2 Solving Equations using MATLAB

The system of nonlinear equations consisting of Eqs. 1–7 are then to be solved in order to determine the value of Ψ_o corresponding to the particular pH value. This system of non-linear equations can be solved using numerical method in MATLAB which invokes an already existing algorithm called trust-region dogleg algorithm [12]. Consider a set of ten pH values, then the algorithm is called ten times to calculate the ten values of Ψ_o. Ψ_o value is necessary for the calculation of threshold voltage of the ISFET device. With the help of [5, 14], we can derived the threshold voltage of the ISFET device as follows:

$$V_{TH} = V_{REF} - \Psi_o + \chi^{sol} + \phi_{ms} - \frac{Q_{ox}}{C_{ox}} + \phi_0 - \frac{Q_B}{C_{ox}} \quad (8)$$

χ_{sol} is the surface dipole potential of the electrolyte solution, ϕ_{ms} is the metal-semiconductor work function difference, V_{REF} is taken as zero while calculating V_{TH}, Q_{ox} is the fixed oxide charge density, ϕ_0 is the value at which Ψ_s is pinned during strong inversion, and Q_B is the depletion region charge density of the semiconductor given by [14]:

$$Q_B = \sqrt{2q\varepsilon_{Si}\varepsilon_0 N_A}\sqrt{\phi_0} \quad (9)$$

After obtaining the threshold voltage the drain current characteristics can be plotted using [14]:

$$I_{DS} = \begin{cases} \mu_n C_{ox}\frac{W}{L}\left[(V_{REF}-V_{TH})V_{DS} - \frac{1}{2}V_{DS}^2\right] & \text{Linear} \\ \frac{1}{2}\mu_n C_{ox}\frac{W}{L}(V_{REF}-V_{TH})^2 & \text{Saturation} \end{cases} \quad (10)$$

The constant parameters used for model development in MATLAB are given in Table 1. The drain current characteristics of the developed analytical model is shown in Fig. 2 with its inset describing the threshold voltage variation w.r.t. the increase in pH value. From Fig. 2, it can be seen that the drain current characteristic shifts towards right as the electrolyte pH value increases linearly from 2 to 12. This is due to the fact that as pH increases the threshold voltage increases correspondingly as seen in the inset. This will be further discussed in Section 4.

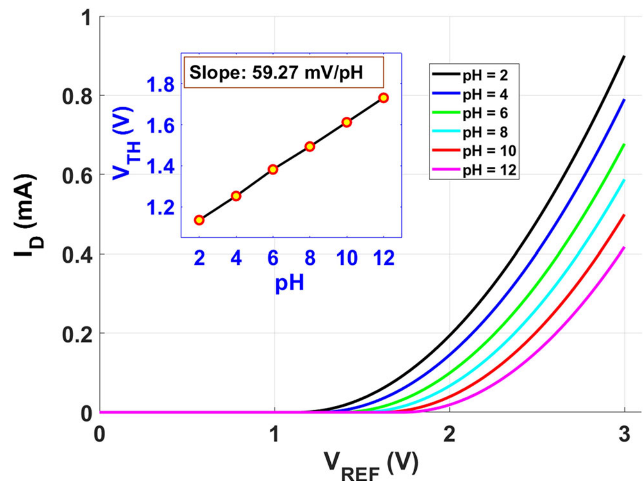

Fig. 2 Drain current characteristics for the numerical model in MATLAB

3 Device Simulation in Synopsys TCAD

Synopsys TCAD is used to simulate the structure given in Fig. 1. TCAD tools do not have any built-in models for an electrolyte material and also for handling electrochemical reactions over an oxide surface [28], hence we exploit its user defined features to observe the structure shown in Fig. 3.

3.1 Electrolyte Modeling

According to [23], we can exploit the similarity between the charge distribution inside an electrolyte and the charge distribution inside a semiconductor. So an intrinsic semiconductor can be modeled to behave as an electrolyte with varying

Table 1 Parameter values used in the MATLAB numerical model

Parameter	Value	Unit	Parameter	Value	Unit
c_o	$10^{-pH} + 10^{-(14-pH)}$	mol/L	ε_{ox}	$3.9\varepsilon_0$	F/m
C_{stern}	20	μ/cm^2	t_{ox}	4*	nm
ε_w	81	1	ε_{Si}	$11.7\varepsilon_0$	F/m
T	300	K	N_A	10^{16}	cm^-3
N_S	5×10^{14}	cm^-2	n_i	1.5×10^{10}	cm^-3
K_a	10^{-6}	mol/L	ϕ_m	5.1**	eV
K_b	10^2	mol/L	χ^{sol}	0.04264***	V

* value taken in such a way that dielectric breakdown does not occur; ** metal work function of gold electrode; and *** value taken from [27]

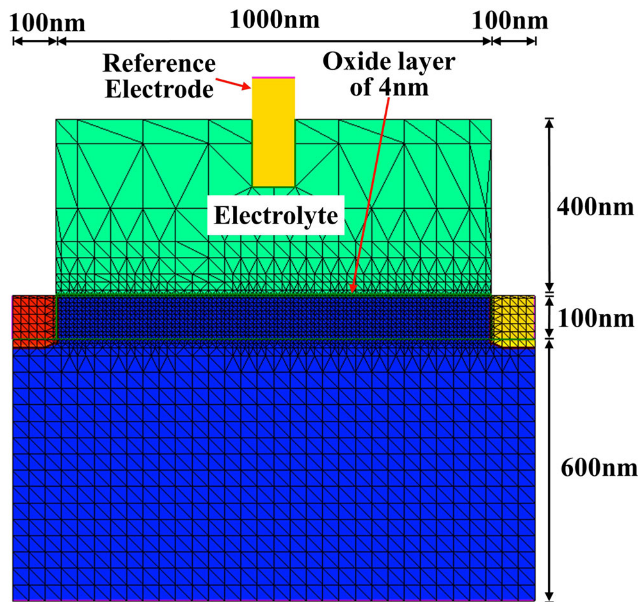

Fig. 3 TCAD simulation

pH values. To do this, the command 'sdevice–P' is used to obtain the default Silicon parameter file and then modifications are made to its critical parameters viz. permittivity, electron affinity, energy bandgap and the density of states.

The relative permitivity of intrinsic semiconductor behaving as the electrolyte is modeled as that of water (which is 80) [16]. According to [25], the electron affinity of the semiconductor (χ_{sol}) can be dtermined in such a way that the V_{TH} vs pH characteristic (in Fig. 5) of the simulated model is closely related to that of the experimental work from [29]. Hence, this value of χ_{sol} is determined to be 2eV. It might be noted that χ_{sol} is not equal to χ^{sol} given in Table 1.

In an electrolyte solution, the Poisson-Boltzmann distribution governs the charge distribution [11] as follows:

$$\frac{\partial^2\Psi}{\partial x^2} = -\frac{q}{\varepsilon}\left[c_o^+ e^{-\frac{q\Psi}{kT}} - c_o^- e^{\frac{q\Psi}{kT}}\right] \tag{11}$$

where c_o^+ and c_o^- are the cation and anion concentrations in the electrolyte, and Ψ is the potential distribution inside the electrolyte. Similarly,a semiconductor is governed by the Fermi-Dirac distribution [17]:

$$\frac{\partial^2\Psi}{\partial x^2} = -\frac{q}{\varepsilon}\left[p_o \frac{1+e^{\frac{E_i-E_v}{kT}}}{1+e^{\frac{E_i-E_v}{kT}} e^{\frac{q\Psi}{kT}}} - n_o \frac{1+e^{\frac{E_c-E_i}{kT}}}{1+e^{\frac{E_c-E_i}{kT}} e^{-\frac{q\Psi}{kT}}}\right] \tag{12}$$

where p_o and n_o are the respective concentratios of hole and electron inside the semiconductor at thermal equilibrium. We then make the two distributions from Eqs. 11 and 12 approximately equal by considering monovalent 1:1 electrolyte, $E_i - E_v = E_c - E_i = E_g/2$ (since the semiconductor is intrinsic), and the energy bandgap to be governed by the following relation [17]:

$$\left(E_g/2 - q\Psi\right) >> kT \tag{13}$$

The bandgap of the Silicon material acting as the electrolyte is set to 6.9eV which is experimentally obtained as an electronic bandgap of water in [21]. The relation stated above in Eq. 13 is also satisfied with this value of E_g.

The pH definition can be included into the semiconductor-acting-as-electrolyte material by exploiting the density of states functions, N_V and N_C. According to Boltzmann statistics [22] the density of states is related to the free electron and hole concentrations by:

$$\begin{cases} N_C \cong n_o e^{\frac{E_c-E_f}{kT}} = n_o e^{\frac{E_g}{2kT}} \\ N_V \cong p_o e^{\frac{E_f-E_v}{kT}} = p_o e^{\frac{E_g}{2kT}} \end{cases} \tag{14}$$

At a particular pH of the electrolyte the number of cations (c_o^+) and anions (c_o^-) available have to be defined as the available free holes (p_o) and electrons (n_o) inside the semiconductor respectively. Hence we can write:

$$\begin{cases} p_o = c_o^+ mol L^{-1} = c_o^+(N_A \times 10^{-3}) cm^{-3} \\ n_o = c_o^- mol L^{-1} = c_o^-(N_A \times 10^{-3}) cm^{-3} \end{cases} \tag{15}$$

where N_A is Avogadro's constant. Since we want to measure the pH of the electrolyte, the cation concentration c_o^+ is taken as the concentration of hydronium ions inside the electrolyte bulk ($[H_3O^+]$) and c_o^- the hydroxide ion concentration ($[OH^-]$). So using the pH formula we get:

$$\begin{cases} c_o^+ = [H_3O^+] = 10^{-pH} \\ c_o^- = [OH^-] = 10^{-(14-pH)} \end{cases} \tag{16}$$

Using Eqs. 15 and 16 in Eq. 14, we get:

$$\begin{cases} N_C = (N_A \times 10^{-3}) \times 10^{-(14-pH)} e^{\frac{E_g}{2kT}} \\ N_V = (N_A \times 10^{-3}) \times 10^{-pH} e^{\frac{E_g}{2kT}} \end{cases} \tag{17}$$

While using the Eq. 17, the following assumption is considered. In practical scenario, at any pH there will always be charge neutrality inside the electrolyte bulk i.e. since we are considering monovalent 1:1 electrolyte, the number of cations and anions will always be equal to maintain charge neutrality. So N_C and N_V are supposed to be equal as seen in Eq. 14. However in our simulation approach we consider the cations to be only hydronium ions and the anions to be only hydroxide ions. For instance, in a low pH HCl acidic solution, the anion concentration (c_o^-) consists of both Cl^- anions and OH^- anions but we consider only the OH^- anions. Similarly in a high pH $NaOH$ alkaline solution the cation concentration (c_o^+) consists of both Na^+ cations and H_3O^+ cations but we consider only the H_3O^+ cations. Hence although N_C and N_V values should be same for a neutral electrolyte solution,

their values are calculated from Eq. 17 according to the electrolyte pH.

3.2 Stern Layer Modeling

The Stern layer described in Fig. 1 is introduced purposely into the simulation model in order to imitate the double layer characteristics. Its thickness is determined by considering the hydroxide anion radius (which is 110pm obtained from [22]) and also the effective hydronium cation radius (obatined from [23]). A dielectric material is used to model the stern layer. Its dielectric constant is determined such that the capacitance of stern layer is $20\mu F/cm^2$ [8] and a thickness of 110pm, resulting in appoximately 2.5.

3.3 Surface Charge Density Modeling

The surface-charge density induced over the surface of oxide layer below the electrolyte is defined by the Site-Binding Model as given in Eq. 4. Since we have modeled the electrolyte solution using an intrinsic semiconductor, we can replace $[H_S^+]$ with the concenntration of hole over the oxide surface, p_s. So Eq. 4 can be written as:

$$\sigma_o = qN_S\left(\frac{p_s^2 - K_aK_b}{p_s^2 + K_aK_b + K_bp_s}\right) \tag{18}$$

Multiplying both numerator and denominator of Eq. 18 by n_s we get:

$$\sigma_o = qN_S\left(\frac{n_sp_s^2 - K_aK_bn_s}{n_sp_s^2 + K_aK_bn_s + K_bp_sn_s}\right) \tag{19}$$

According to the mass action law of semiconductor under thermal equilibrium, we have: $n_i^2 = n_op_o$, where n_o is free electron concentration, p_o is free hole concentration, and n_i is the intrinsic carrier concentration. The relation between the carrier concentration over the oxide surface and the carrier concentration in the electrolyte bulk is given by:

$$n_sp_s = \left(n_oe^{\frac{q\Psi}{kT}}\right)\left(p_oe^{-\frac{q\Psi}{kT}}\right) = n_op_o = n_i^2 \tag{20}$$

Using Eqs. 20 in 19, we get:

$$\sigma_o = qN_S\left(\frac{n_i^2p_s - K_aK_bn_s}{n_i^2p_s + K_aK_bn_s + K_bn_i^2}\right) \tag{21}$$

To find the value of n_i^2, we consider the equilibrium reaction that takes place in water, i.e. $H_2O \xleftrightarrow{K_w} H_3O^+ + OH^-$, where K_w is the water dissociation constant. According to the mass action law of pure water at standard temperature and pressure, K_w is defined [15] by: $K_w = [H_3O^+][OH^-]$. This relation is similar to the semiconductor mass action law and hence we consider n_i^2 to be equal to K_w as: $n_i^2 = \left(N_A10^{-3}\right)^2 K_w$, where $\left(N_A10^{-3}\right)$ is used to convert mol/L to cm^{-3}.

From (21), it can be seen that the surface charge density, σ_o depends explicitly on the local concentrations of charge carriers, n_s and p_s over the oxide surface. This relation can be easily evaluated using TCAD tools. Another critical consideration made in our approach is that, practically, the oxide surface binds to cations and anions depending on the electrolyte pH. However a double layer (DL) appears on the oxide surface due to the finite size of the cations and the anions which are bound onto the oxide surface. So we can consider that the oxide surface charge density apparently exists on the outer surface of the stern layer (first layer of DL). To mimic this nature of oxide surface, the interface traps between the stern layer and the electrolyte material are manipulated using user-defined interface trap models by modifying the capture and emission rates of each trap type.

Synopsys TCAD uses the following in-built equation for the interface trap charge density, σ_T [16, 24]:

$$\sigma_T = q\left(N_S^df^d - N_S^af^a\right) \tag{22}$$

where N_S^a and N_S^d are the acceptor trap density and donor trap density respectively, and f^a and f^d the acceptor trap occupation probability and the donor trap occupation probability respectively, given by [16, 24]:

$$\begin{cases} f^a = \frac{c_C^a + c_V^a}{c_C^a + c_V^a + e_C^a + e_V^a} \\ f^d = \frac{c_C^d + c_V^d}{c_C^d + c_V^d + e_C^d + e_V^d} \end{cases} \tag{23}$$

where c_C and c_V are the capture rates of conduction band and valence band respectively, while e_C and e_C are the emission rates of conduction band and valence band respectively. For the purpose of simplification [16, 28], the donor traps (or acceptor traps) are considered to exchange charge carriers only with the valence band (or conduction band) of the semiconductor-acting-as-electrolyte i.e. $c_C^d = c_V^a = e_C^d = e_V^a = 0$. Using this assumption in Eqs. 23, 22 can be written as:

$$\sigma_T = q\left(N_S^d\frac{c_V^d}{c_V^d + e_V^d} - N_S^a\frac{c_C^a}{c_C^a + e_C^a}\right) \tag{24}$$

In order to make the interface trap charge density imitate the oxide surface charge density due to the electrolyte, we need to map (24) to (21) as follows:

$$\begin{cases} N_S^d = N_S^a = N_S \\ c_V^d = n_i^2p_s \\ c_C^a = K_aK_bn_s \\ e_V^d = K_aK_bn_s + K_bn_i^2 \\ e_C^a = n_i^2p_s + K_bn_i^2 \end{cases} \tag{25}$$

To achieve this, first we introduce the donor and acceptor trap densities ($N_S^d = N_S^a = N_S$) into the sdevice physics section. Now to change the default formulae of the capture and the emission rates (c_C^a, c_V^d, e_C^a and e_V^d) of the interface

Table 2 PMI model parameters

Parameter	Value	Unit
N_S	5×10^{14}	cm^{-2}
K_a	10^{-6}	mol/L
K_b	10^{2}	mol/L
n_i^2	10^{-14}	$(mol/L)^2$

traps, an advanced feature of TCAD Synopsys called the Physical Model Interface (PMI) is exploited. Using PMI we first write C^{++} functions to compute the capture and emission rates for the donor and the acceptor trap sites. Then we compile the source-code files into shared object files using a version of gcc compiler known as cmi. After this we provide the path of these PMI models in the sdevice file section. These shared object files will be loaded by the Sentaurus at run-time using the dynamic loader [24] and the user defined models will then be used instead of the default models provided by the Synopsys TCAD. The parameters used in the PMI models are listed in Table 2.

3.4 Device Simulation

Other than the user-defined models discussed in the above sections, two additional built-in physical models for mobility and bandgap narrowing are used during the simulation. The mobility models include DopingDep denoting the doping dependence model and Enormal denoting the transverse field model. During simulation, these models are used to calculate the carrier mobility at each mesh node inside the channel [28]. During I_D calculation, DopingDep model considers the carrier density developed as a result of dopant concentration; and Enormal model considers the induced transverse electric field resulting from the reference voltage and also as a result of the electrolyte pH [28]. The intrinsic carrier concentration inside the semiconductor (both silicon and

Table 3 Device parameters

Parameter	Value	Unit
N_D *of source*	1e20	cm^{-3}
N_D *of drain*	1e18	cm^{-3}
N_A *of channel and body*	1e16	cm^{-3}
Channel length	1000	nm
Oxide thickness	4	nm
Stern layer thickness	0.11	nm
Electrolyte thickness	400	nm

electrolyte materials) is governed by the bandgap narrowing model. Considering the above models and techniques, the structure given in Fig. 1 is simulated as shown in Fig. 3, and its device parameters are listed in Table 3.

Among the device parameters given in Table 3, the stern layer thickness of 0.11nm is determined according to Section 3.2. The other parameters viz. doping concentrations, channel length, oxide thickness and electrolyte thickness are determined for a conventional long channel bulk-MOSFET in such a way that the V_{TH} vs pH curve from TCAD simulation approaches very close to those obtained from MATLAB modeling and experimental data as shown in Fig. 5 under model validation section. These parameters are determined such that dielectric breakdown and short channel effects do not significantly affect the drain current characteristics given in Fig. 4.

Figure 4a describes the drain current characteristics for various pH values. In this figure we observe that the characteristic shifts towards right as pH increases, which is quite similar to the behaviour described in Fig. 2. This is because as pH increases, the inversion layer in the channel decreases and the amount of V_{REF} needed to maintain the same level of inversion layer increases accordingly. This is evident from the inset of Fig. 4b where V_{TH} increases almost linearly with increase in pH.

Hence we can say that the pH of the electrolyte modulates the threshold voltages thereby affecting the drain current characteristics of the ISFET device. The threshold voltages are obtained using constant current method as explained in [26, 28], where the V_{REF} value of each pH curve is measured at $I_D = 10^{-7}A$ which makes the simulation results closest to the experimental data. Using a proper readout circuit for the threshold voltage as in [29], any change in the pH of the electrolyte solution can be detected.

From 4b, it is observed that the ON current: $I_{ON} \approx 10^{-4}$ A when V_{REF} = 3V and V_{DS} = 0.5V. Similarly the OFF current: $I_{OFF} \approx 10^{-17}$ A when V_{REF} = 0V and V_{DS} = 0.5V. The current ratio is 10^{13}. A current ratio of 10^{13} would mean good suitability in digital applications. The underlying MOSFET structure in this ISFET device is a long channel (1000nm) bulk-MOS, so V_{DS} = 0.5V is not adequate enough to cause any notable leakage power dissipation while V_{GS} = 0V. Moreover the doping concentrations given in Table 3 are determined through repeated simulations in such a way that no considerable short channel effect comes to exist. Hence we obtain very low I_{OFF} current in the proposed ISFET device. It is also observed that the subthreshold swing is 66.51mV/dec. Due to the effect of bulk in conventional MOSFET, the subthreshold swing (SS) will always be larger than an optimum value of around 60 mV/dec, taken at room temperature. A small subthreshold swing is desired

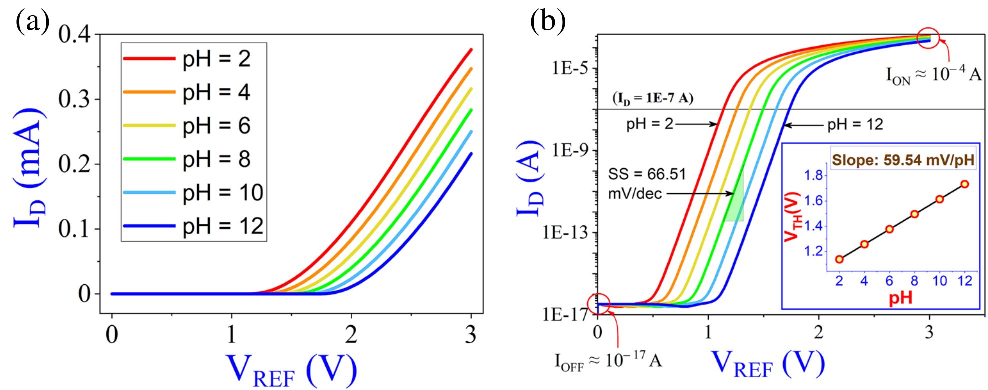

Fig. 4 (a) Resulting drain current characteristics for pH = 2 to 12. V_{DS} = 0.5V, V_B = 0V. (b) Extraction of threshold voltages using constant current method [26]. The inset describes the V_{TH} vs pH curve

as it improves the I_{ON}/ I_{OFF} ratio, induces less leakage and less energy, and a better performance. Small SS dictates that the bulk charge in depletion region under the channel region changes as small as possible when V_{GS} varies. This proposed work approaches 60mV/dec, hence the device has a good performance although it cannot be compared to advanced devices.

3.5 Model Validation

To check the validity of our simulation approach, Fig. 5 compares the simulation sensitivity of 59.54 mV/pH obtained from Fig. 4b with the experimental one of 58 mV/pH from [29] and also w.r.t. the theoretical reference of 59.27 mV/pH from Fig. 2. Figure 5 shows that the simulation model is in close agreement with the experimental model and also with the theoretical reference.

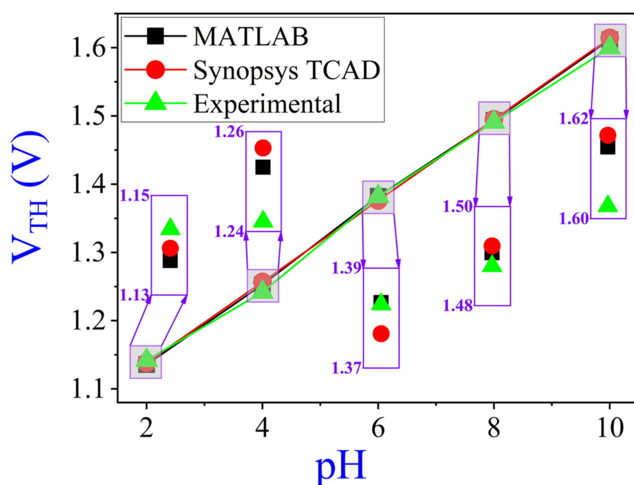

Fig. 5 Comparison of V_{TH} vs pH characteristics for the three types of model—Numerical, Simulation and Experimental

The error observed in the sensitivity of the simulation model is around 2.66% w.r.t. the experimental data and around 0.46% w.r.t. the theoretical reference. So it can be inferred from the above statistics that both the built-in and the user-defined models used during the simulation of the ISFET pH sensor in TCAD are valid.

Andrea Bandiziol et al. [16] modeled a simple bulk-MOS ISFET where N_C and N_V are taken same according to practical scenario and also the site binding reactions are modeled between the stern layer and the oxide as in theoretical sense which posed its own certain difficulty. In our proposed work, N_C and N_V are considered to be different as in an ideal pH solution and the site binding reactions are modeled between the stern layer and the electrolyte which makes the simulation more practical-like. Our work explicitly uses experimental data from various literatures during the simulation. Daniel Passeri et al. [22] modeled a simple bulk-MOS ISFET without the stern layer and proceeds to design a Bio-FET device where they have considered charge localizations using dielectric blocks on top of the oxide surface, whereas our work considers interface trap modeling with random localizations over the oxide surface. We were also able to achieve high I_{ON}/I_{OFF} ratio. This model can be upgraded to double-gated device to increase the sensitivity as discussed in [28].

4 Results and Discussion

4.1 Electrostatic potential

The change in electrostatic (or electric field) potential can be observed from Fig. 6. As pH increases, the effective potential available over the oxide surface reduces. Due to this the strength of electric field induced towards the channel decreases. This is indicated by the colour plot used in the figure.

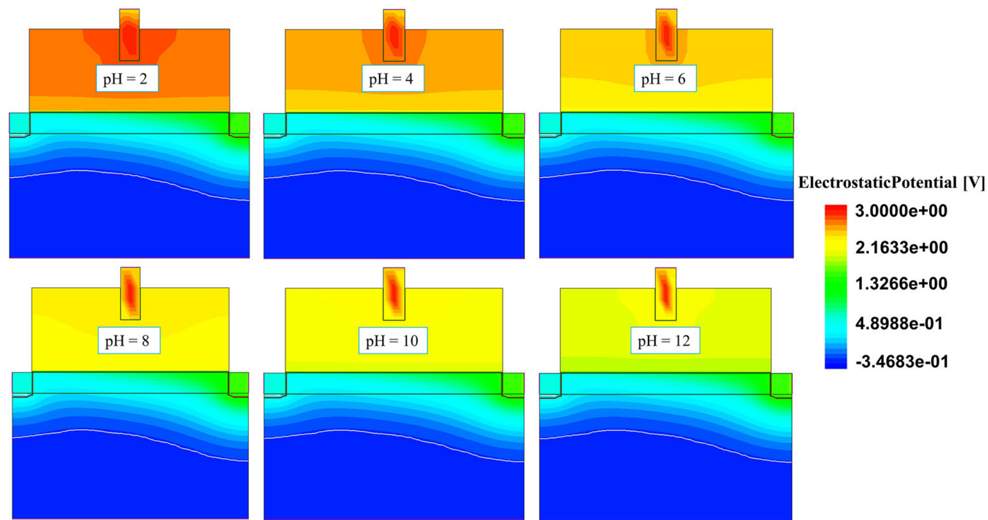

Fig. 6 Change in electrostatic potential as pH increases. V_{REF} = 3V

4.2 Interface Traps

As pH increases the concentration of H_3O^+ ion decreases while the concentration of OH^- ion increases. Figure 7 depicts the change in probability of trap occupation at the electrolyte/oxide interface w.r.t. change in pH. Figure 8 describes the resulting trapped carrier density at the interface due to the change in probability of trap occupation.

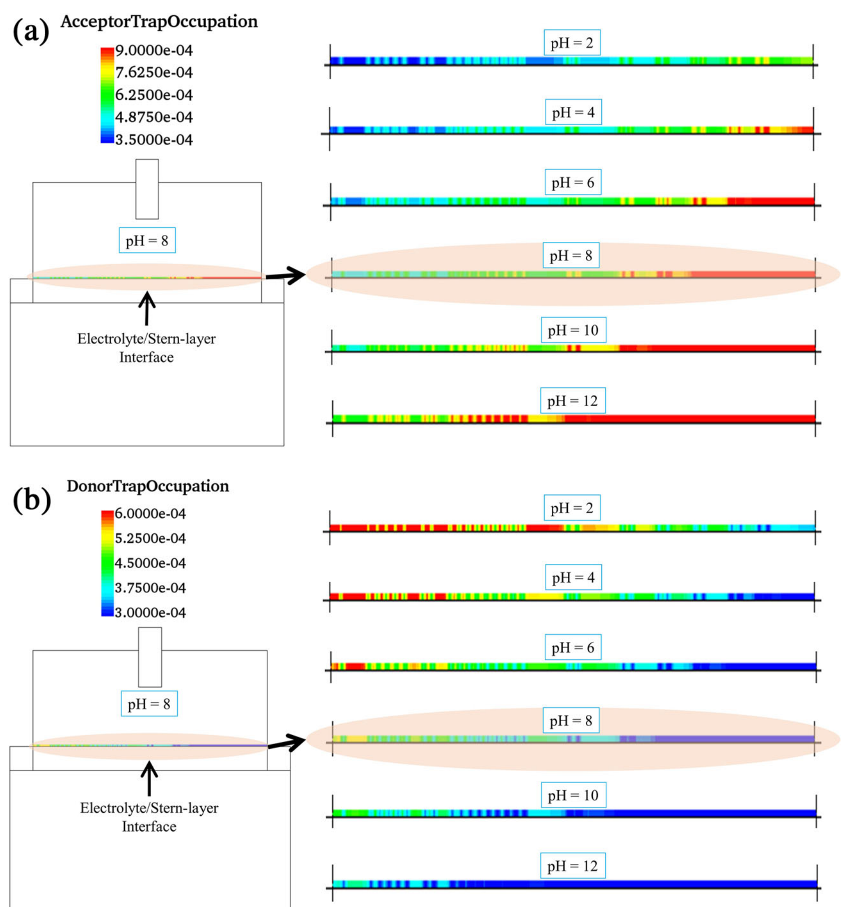

Fig. 7 Probability of (a) Acceptor Trap Occupation (b) Donor Trap Occupation. As pH increases more acceptor traps are getting occupied while more donor traps are getting unoccupied. V_{REF} = 3V

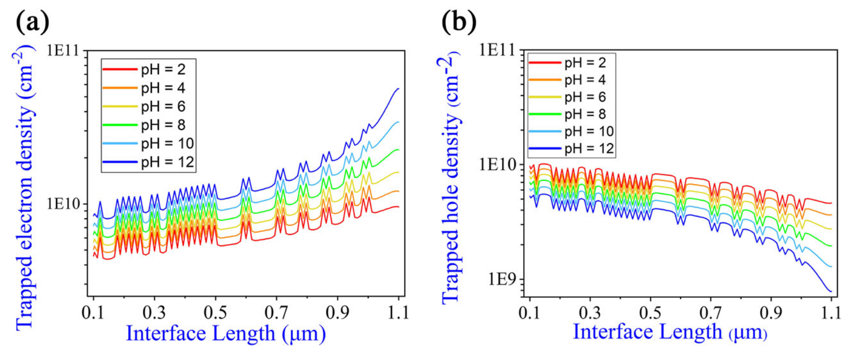

Fig. 8 (a) Density of interface trapped electrons. (b) Density of interface trapped holes. As pH increases electrons are getting readily trapped at the interface while trapped holes are getting released

To ensue current conduction through the device channel, the source is grounded while the drain is given a positive voltage. As a result, at a particular pH the acceptor traps near the drain side require lesser energy to accept electrons, thereby increasing the probability of acceptor trap occupation as seen in Fig. 7a. Similarly the donor traps near the drain side require more energy to donate electrons or capture holes, thereby decreasing the probability of donor trap occupation as seen in Fig. 7b. It is observed that the curves in Fig. 8 exhibit a noise-like waveforms. This is due to the random distribution of interface traps specified in the sdevice tool.

4.3 Inversion Layer

From Fig. 6 it is observed that as pH increases, the effective potential available over the oxide surface reduces due to which electrons have lesser tendency to be pulled towards the channel resulting in thinner inversion layer. This change is illustrated in Fig. 9a. The corresponding change in the charge density developed at the inversion layer is shown in Fig. 9b. Due to this effect, the drain current characteristic is modulated by the change in pH as seen in Figs. 2 and 4a.

5 Conclusion

A compact analytical model has been put together from various literature surveys to describe the physics of an ISFET device corresponding to a pH-sensor. A simulation study is conducted using Synopsys TCAD tool with exclusive reference to various experimental data. This article explains the reason behind the consideration of $N_C \neq N_V$ during electrolyte modeling and also demonstrates how the stern layer modeling can be simplified by considering the oxide surface charge density at the electrolyte/stern-layer interface. A sensitivity value of 59.54 mV/pH is achieved, which is accurate as compared to the experimentally obtained value of 58mV/pH from [29] and is also quite close to the theoretical reference of 59.27 mV/pH in MATLAB. We believe that this article can be quite helpful to readers who wish to have a quick understanding of the ISFET mechanism and its TCAD simulation techniques.

The difference in the considerations of room temperature at 300K during TCAD simulation against that of 298K in experimental work might have led to a small amount of deviation in the sensitivity value. The sensitivity of ISFET device can be further increased using the amplification

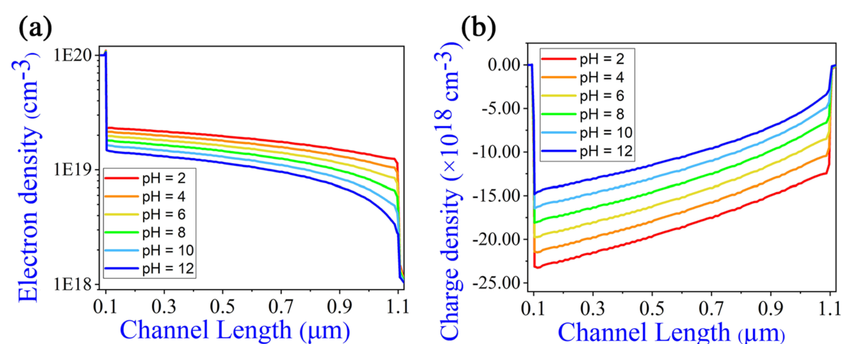

Fig. 9 (a) Electron density at the inversion layer. (b) Charge density at the inversion layer. As pH increases the inversion layer thickness decreases resulting in the charge density getting less negative.

characteristic of double-gate FET structure. To simulate the various selectivities of the sensor, advanced research into the TCAD user-defined features still needs to be done, which is beyond the scope of this article.

Author Contributions Contributions of each author have all been accounted.

Data Availability The authors declare that the data supporting the findings of this study are available within the article.

Declarations

Ethics approval Authors guidelines have been maintained.

References

1. Bergveld P (1970) Development of an ion-sensitive solid-state device for neurophysiological measurements. IEEE Trans Biomed Eng BME-17(1):70–71. https://doi.org/10.1109/TBME.1970.4502688
2. Bergveld P (2003) Thirty years of ISFETOLOGY, What happened in the past 30 years and what may happen in the next 30 years. Sens Actuators B 88(1):1–20. https://doi.org/10.1016/S0925-4005(02)00301-5
3. Sukesan R, Chen YT, Shahim S, Wang SL, Sarangadharan I, Wang YL (2019) Instant mercury ion detection in industrial waste water with a microchip using extended gate field-effect transistors and a portable device. Sensors 19(2209). https://doi.org/10.3390/s19092209
4. Joly M, Mazenq L, Marlet M, Temple-Boyer P, Durieu C, Launay J (2017) All-solid-state multimodal probe based on ISFET electrochemical microsensors for in-situ soil nutrients monitoring in agriculture
5. Yates DE, Levine S, Healy TW (1974) Site-binding model of the electrical double layer at the oxide/water interface. J Chem Soc, Faraday Trans 1, Phys Chem Condens Phases 70:1807–1818. https://doi.org/10.1039/F19747001807
6. Bergveld P (2003) ISFET, theory and practice. In: IEEE sensor conference, Toronto, vol 10
7. van der Schoot BH, Bergveld P (1987) ISFET based enzyme sensors. Biosensors 3:161–186. https://doi.org/10.1016/0265-928X(87)80025-1
8. Kosmulski M (1995) Oxide/electrolyte interface: electric double layer in mixed solvent systems. Colloids Surf A 95:81–100. https://doi.org/10.1016/0927-7757(94)03029-Y
9. van Hal REG, Eijkel JCT, Bergveld P (1996) A general model to describe the electrostatic at electrolyte oxide interfaces. Adv Colloid Inter Sci 69(1-3):31–62. https://doi.org/10.1016/S0001-8686(96)00307-7
10. Grattarola M, Massobrio G, Martinoia S (1992) Modeling H/sup +/-sensitive FETs with SPICE. IEEE Trans Electron Dev 39(4):813–819. https://doi.org/10.1109/16.127470
11. David CG (1947) The electrical double layer and the theory of electro-capillarity. Chem Rev 41(3):441–501. https://doi.org/10.1021/cr60130a002
12. MATLAB (March 2017) Equation solving algorithms, version R2017a, Natick, Massachusetts, The MathWorks Inc.
13. Bard AJ, Faulkner LR (2001) 13 Electrochemical Methods Fundamentals and Applications, 2nd edn. Wiley, New York
14. Tsividis Y, McAndrew C (2004) Operation and Modelling of the MOS Transistor. Oxford Univ Press, London
15. Peech M (1965) Hydrogen-ion activity. In: Methods of Soil Analysis, John Wiley & Sons, Ltd., ch. 60, pp 914–926
16. Bandiziol A, Palestri P, Pittino F, Esseni D, Selmi L (2015) A TCAD-based methodology to model the site-binding charge at ISFET/electrolyte interfaces. IEEE Trans Electron Dev 62(10):3379–3386. https://doi.org/10.1109/TED.2015.2464251
17. Chung I-Y, Jang H, Lee J, Moon H, Seo SM, Kim DH (2012) Simulation study on discrete charge effects of SiNW biosensors according to bound target position using a 3D TCAD simulator. Nanotechnology 23(6):065202. https://doi.org/10.1088/0957-4484/23/6/065202
18. Dinar AM, Zain ASM, Salehuddin F, Mothana LA, Abdulhameed MK, Mowafak KM (2019) Modeling and simulation of electrolyte pH change in conventional ISFET using commercial Silvaco TCAD. In: IOP Conference series: materials science and engineering, vol 518, p 042020. https://doi.org/10.1088/1757-899x/518/4/042020
19. Marcus Y (2012) Volumes of aqueous hydrogen and hydroxide ions at 0 to 200°. J Chem Phys 137(15):154501. https://doi.org/10.1063/1.4758071
20. Wang X, Bommier C, Jian Z, Li Z, Chandrabose RS, Rodríguez-Pérez IA, Greaney PA, Ji X (2017) Hydronium-ion batteries with perylenetetracarboxylic dianhydride crystals as an electrode. Angew Chem Int Ed Engl 56(11):2909–2913. https://doi.org/10.1002/anie.201700148
21. Coe JV, Earhart AD, Cohen MH, Hoffman GJ, Sarkas HW, Bowen KITH (1997) Using cluster studies to approach the electronic structure of bulk water: Reassessing the vacuum level, conduction band edge, and band gap of water. J Chem Phys 107:6023–6031. https://doi.org/10.1063/1.474271
22. Passeri D, Morozzi A, Kanxheri K, Scorzoni A (2015) Numerical simulation of ISFET structures for biosensing devices with TCAD tools. BioMed Eng OnLine 14:1–16. https://doi.org/10.1186/1475-925X-14-S2-S3
23. Pittino F, Palestri P, Scarbolo P, Esseni D, Selmi L (2014) Models for the use of commercial TCAD in the analysis of silicon-based integrated biosensors. Solid-State Electron 98:63–69. https://doi.org/10.1016/j.sse.2014.04.011
24. SentaurusTM Device User Guide (2015) Synopsys, Mountain View, CA, USA
25. Narang R, Saxena M, Gupta M (2017) Analytical model of pH sensing characteristics of junctionless silicon on insulator ISFET. IEEE Trans Electron Dev 64(4):1742–1750. https://doi.org/10.1109/TED.2017.2668520
26. Liou JJ, Ortiz-Conde A, Garcia-Sanchez F (1998) Extraction of the threshold voltage of MOSFETs. In: Analysis and design of mosfets. Springer, Boston. https://doi.org/10.1007/978-1-4615-5415-8_3
27. Bhardwajn R, Sinha N, Sahu S, Majumder P, Narang RM (2019) Modeling and simulation of temperature drift for ISFET based pH sensor and its compensation through machine learning techniques. Int J Circuit Theory Appl 47(6):954–970. https://doi.org/10.1002/cta.2618
28. Khwairakpam DS, Pukhrambam PD (2021) Sensitivity optimization of a double-gated ISFET pH-sensor with HfO_2/SiO_2 gate dielectric stack. Microelectronics J 118:105282. https://doi.org/10.1016/j.mejo.2021.105282
29. Chin Y-L, Chou J-C, Sun T-P, Chung W-Y, Hsiung S-K (2001) A novel pH sensitive ISFET with on chip temperature sensing using CMOS standard process. Sens Actuators B 76(1):582–593. https://doi.org/10.1016/S0925-4005(01)00639-6

Publisher's Note Springer Nature remains neutral with regard to jurisdictional claims in published maps and institutional affiliations.